ELSEVIER

Journal of Magnetism and Magnetic Materials 249 (2002) 300–304

journal of magnetism and magnetic materials

www.elsevier.com/locate/jmmm

The analysis of magnetoimpedance by equivalent circuits

R. Valenzuela*

Institute for Materials Research, National University of Mexico, P.O. Box 70-360, Mexico, D.F., 04510, Mexico

Abstract

Simple circuits formed by resistors, inductors and capacitors can be used to model giant magnetoimpedance (GMI) with a good approximation. Three different circuits are found to represent GMI in the whole frequency range (100 Hz–9 GHz) and the AC magnetic field amplitude range (0.01–7.22 A/m RMS): a series $R_sC_sL_s$, a parallel R_pL_p and a parallel R_HL_H, associated with the magnetization processes of spin rotation (leading to ferro-magnetic spin resonance), domain wall bulging (initial permeability) and domain wall displacement (magnetic hysteresis), respectively. We also propose a correlation between these elements and physical parameters of the sample, such as permeabilities, domain wall damping parameters and domain wall effective mass.

Keywords: Magnetoimpedance; Equivalent circuits

1. Introduction

Giant magnetoimpedance (GMI) has generated a strong interest due to both its technological applications [1–3], as well as to the basic physics involved in the phenomenon [4,5]. Some recent studies have used the complex permeability formalism with the aim of investigating the dependence of GMI on magnetization processes, especially for the low frequency case ($f < 5$ MHz). Results can be interpreted in terms of spin rotation, bulging of pinned domain walls and domain wall displacements [6–8].

In this paper, we propose the use of equivalent circuits (EC) to model the GMI response of as-cast amorphous ferromagnetic wires. We show that there is an association between EC and magnetization processes, as well as a correlation between EC elements and physical parameters of the sample.

2. Experimental techniques

We used a measuring system including an HP 4192 A impedance analyzer controlled by a PC, described elsewhere [9]. The software, created in our laboratory, allows the measurement of 94 different frequencies in the frequency range 100 Hz–13 MHz in less than 3 min. The experiments were carried out on as-cast amorphous wires of nominal composition $(Co_{94}Fe_6)_{72.5}B_{15}Si_{12.5}$, prepared by the in-water-rotating technique [10], kindly provided by Unitika Ltd., Japan. These wires are of 125 μm in diameter. Measurements were carried out at room temperature on pieces 6–10 cm long.

*Fax: +52-55-6161371.
E-mail address: monjaras@servidor.unam.mx (R. Valenzuela).

0304-8853/02/$ - see front matter
PII: S0304-8853(02)00547-4

3. Experimental results and equivalent circuits

We measured the total impedance, $Z_t[Z_t^2 = (Z')^2 + (Z'')^2]$, with its real, Z', and imaginary, Z'', contributions to the complex impedance, $\mathbf{Z}, [\mathbf{Z} = Z' + jZ'']$, where j is the basis of the imaginary numbers, $j = \sqrt{-1}$.

To get more insight into the magnetization phenomena it is necessary to change from the complex impedance formalism to the complex permeability formalism. On the basis of an electric circuit approach, we first transform complex impedance into complex inductance by means of $\mathbf{L} = -(j/\omega)\mathbf{Z}$, where $\mathbf{L}$ is the complex inductance, formed by the real and imaginary contributions, $\mathbf{L} = L' + jL''$, and ω is the angular frequency ($\omega = 2\pi f$).

If we consider now the low frequency case, where the skin depth is larger than the radius of the wire, the permeabilities can be straightforwardly determined from inductance by a geometrical factor G, $\boldsymbol{\mu} = G\mathbf{L}$, where $\boldsymbol{\mu} = \mu' - j\mu''$, and for the case of cylindrical geometry [11], $G = 10^8/\boldsymbol{l}$ (with $\boldsymbol{l}$ in m). This relationship can be obtained also in a rigorous physical basis by considering the expression of impedance in terms of Bessel functions [12].

Measurements of the real permeability as a function of frequency at zero DC magnetic field, H_{DC}, and a saturating field of 6.4 kA/m (80 Oe) (Fig. 1) showed clear differences. These measurements were carried out at an amplitude of AC current of 1 mA (RMS), and showed no difference for smaller AC current amplitudes. At zero field, μ' shows a low frequency plateau up to $\sim$10 kHz, followed by a decrease (a dispersion) as frequency increases. At high frequencies, μ' shows the tendency to a small, constant value. Results at the high DC applied field, on the other hand, exhibited a virtually constant value on all this frequency range; μ' tends to become the same constant for both cases at high frequencies. The imaginary part of permeability for these two cases (zero and saturating DC field) is shown in Fig. 2. At low frequencies, the DC applied field leads to no difference between the two cases; at high frequencies, the zero field results increase and deviate from a $\sim(-1)$ slope.

A very useful representation when dealing with circuits is the complex plane, also known as Cole–Cole plot, where the imaginary part is plotted as a function of the real part. Each point is therefore obtained for a given frequency. Typically, a "spike" (a vertical variation where the real part is constant) is associated with a series *RL* circuit; a semicircle with a parallel *RL* (relaxation) circuit [8]; and a full circle with a (resonant) *RCL* circuit. This representation appears in inset of Fig. 2, showing a "spike" for the high field case. A complex behavior is observed for the zero field condition, including a section with a spike.

From an electric circuit analysis, we should start by considering the two simplest circuits for magnetic (i.e., inductive) elements: series *RL* and parallel *RL*. It can be shown that the equations for

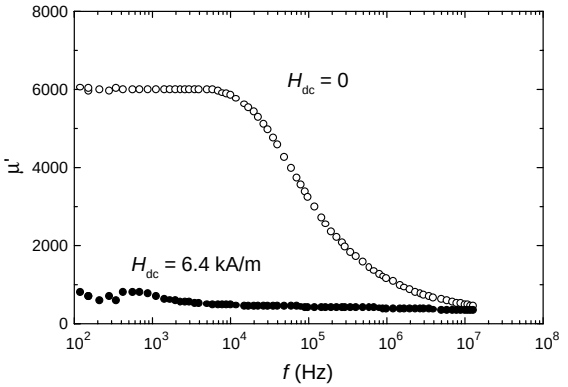

Fig. 1. Real part of permeability at $H_{DC} = 0$ and 6.4 kA/m.

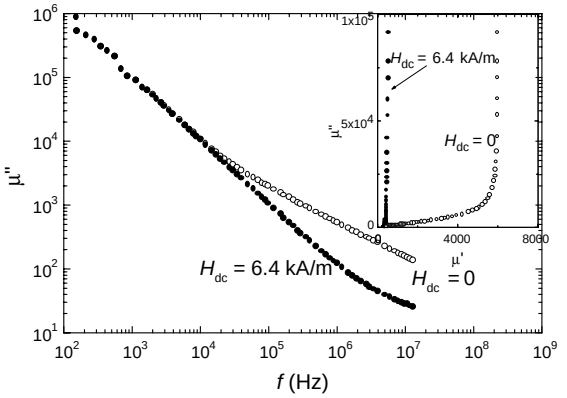

Fig. 2. Imaginary part of permeability at $H_{DC} = 0$ and 6.4 kA/m. In inset, the Cole–Cole plot.

real and imaginary permeabilities for an RL series circuit can be written as $\mu' = GL$, and $\mu' = GR/\omega$, respectively (where R and L are ideal resistor and inductor elements). For an RL parallel circuit, $\mu' = G\,R\omega L^2/(R^2 + \omega^2 L^2)$, and $\mu'' = GR^2L/(R^2 + \omega^2 L^2)$.

By inspecting the experimental results, we could say that the high DC field behavior can be modeled by means of the series arrangement, since μ' showed a constant behavior (G, R and L are both independent of f) in Fig. 1, μ'' exhibited a (-1) slope as a function of frequency in Fig. 2, and a "spike" also in inset of Fig. 2. The results at $H_{DC} = 0$ are more difficult to assess, but we could expect that the modeling circuit has an RL parallel section, since μ' exhibited a clear relaxation in Fig. 1.

In order to progress in this analysis, we propose the following assumption: the equivalent circuit at $H_{DC} = 0$ is a combination of a parallel R_pL_p circuit and a series R_sL_s circuit, connected in series. The effect of the saturating DC applied field is then to eliminate the parallel R_pL_p arm, leaving only the series part. In order to confirm this assumption, we make a subtraction of experimental results obtained for the $H_{DC} = 6.4\,\mathrm{kA/m}$ case, from the $H_{DC} = 0$ condition, as follows:

$$\Delta\mu' = \mu'(H_{DC} = 0) - \mu'(H_{DC} = 6.4\,\mathrm{kA/m}), \quad (1)$$

$$\Delta\mu'' = \mu''(H_{DC} = 0) - \mu''(H_{DC} = 6.4\,\mathrm{kA/m}). \quad (2)$$

This calculation, carried out point-to-point for each frequency, can be represented in terms of equivalent circuits as: {series + parallel} − {series} = {parallel}. To confirm this, we expect that the resulting plots have all the characteristics of a parallel R_pL_p circuit: a relaxation in μ', a maximum in μ'', and a semicircle in the Cole–Cole plot. It can be shown that the relaxation frequency in such a parallel circuit appears when the impedances in both arms become equal. For the resistive part the impedance is simply $\mathbf{Z}_R = R_p$, while for the inductor section it is $\mathbf{Z}_L = \omega L_p$; if $\mathbf{Z}_R = \mathbf{Z}_L$ which leads to $\omega_x = R_p/L_p$. The result of the operation in Eqs. (1) and (2) is shown in Fig. 3 (with the Cole–Cole plot in inset), and confirm our assumption. It is now important to provide a physical basis which could explain the association

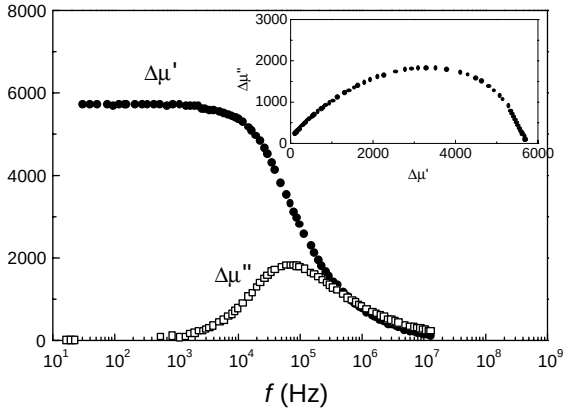

Fig. 3. Real and imaginary permeabilities resulting form the subtraction of Eqs. (3) and (4). In inset, the Cole–Cole plot.

of these equivalent circuits with the observed results. To be of any use, a valid equivalent circuit should allow a direct association of elements with physical parameters of the sample. In particular, it would be useful to find what magnetization processes can be represented by means of the two circuits: a series R_sL_s, and a parallel R_pL_p.

4. Magnetization processes

The use of equivalent circuits have shown that at low f, there are two magnetization processes. One of the processes is characterized by high permeability values ($\mu \sim 6000$ at extremely low amplitude of AC fields) independent of the AC field amplitude (in the 0.1–1.0 mA RMS), a relaxation dispersion with $\omega_x \approx 100\,\mathrm{kHz}$, and also by the fact that it is strongly damped by the DC field. These factors point to a process based on domain wall movements, and we proposed [6] the bulging of pinned domain walls (initial permeability).

The other process possess a smaller permeability value (about ~ 500) also independent of the AC field amplitude, and do not show a dispersion in the frequency range investigated. We have proposed spin rotation [6] to explain these results. In the case of this circuit, recent experimental results have shown that at high frequencies in GHz range, ferromagnetic resonance is observed [12,13], which

confirms that this process is effectively spin rotation. This means that we should add a capacitor C_s, probably in parallel with the inductor L_s to represent the equivalent circuit (to our knowledge, the exact equivalent circuit for ferromagnetic resonance as observed from GMI measurements has not been established). The experimental results obtained in Figs. 1 and 2 can therefore be interpreted as corresponding to the contribution of both magnetization processes, up to ~ 1 MHz, where domain wall bulging becomes unable to follow the excitation field; for frequencies above this value, only spin rotation remains as active process. These measurements allow a resolution (separation) of the magnetization processes on the basis of their dynamics (time-constant). The subtraction operation we carried out in Eqs. (3) and (4) eliminated the contribution of spin rotation and left only the domain wall bulging process. This subtraction eliminated also the DC resistance.

The classic equation of motion can be useful to find a relationship between the equivalent circuit elements and some physical parameters of the material. This equation is expressed as

$$m\,\mathrm{d}^2z/\mathrm{d}t^2 + \beta \mathrm{d}z/\mathrm{d}t + \alpha z = F(t). \quad (3)$$

Here, $m\,\mathrm{d}^2z/\mathrm{d}t^2$ is the inertia term, with m being the effective mass, z is the displacement, $\beta\,\mathrm{d}z/\mathrm{d}t$ is the damping term, where β is the (viscous) damping coefficient, αz is the restoring term (α is the restoring coefficient) and $F(t)$ is the excitation force driving the system.

When the inertia term is very small and negligible as compared with the other terms, and the system is driven by a periodic force ($F(t) = A_0 \exp(\mathrm{j}\omega t)$, with j is the basis of imaginary numbers, ω the angular frequency), Eq. (1) simplifies and can be solved to obtain the relaxation frequency, $\omega_x = \alpha/\beta$, where ω_x is the relaxation frequency. In spectroscopic plots (plotting as a function of frequency), relaxation is characterized by a decrease in the real part of the polarization, while the imaginary contribution exhibits a maximum, as shown in Fig. 4. The so-called Cole–Cole, or complex plots, where the imaginary part appears as a function of the real part, can be very useful in such simple cases, since the locus of points for a relaxation process leads to semicircle, inset of Fig. 3, and can then be easily identified.

A resonance dispersion is characterized by the fact that the inertia term is important as compared with the other terms. The solution to Eq. (3) is in this case becomes, $\omega_s = (\alpha/m)^{1/2}$, where ω_s is the resonance frequency. The locus of the points in the Cole–Cole plot is a full semicircle, as the one observed in Refs. [12,13].

All the previous results were obtained at low AC field amplitudes, h_{AC}. The variations in the AC current amplitude (which leads to variations in the AC field amplitude) have been analyzed [6]. An interpretation consistent with all the results here presented has been proposed, in terms of a threshold field or propagation field, which represents the point where domain walls are unpinned and displaced. A second $R_H L_H$ parallel circuit should be considered, to model the domain wall displacement process, as shown in Fig. 4. Finally,

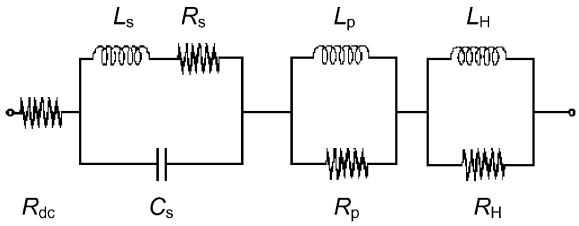

Fig. 4. Total equivalent circuit showing all the magnetization processes: spin rotation ($R_sL_sC_s$), bulging of pinned domain walls (R_pL_p) and domain wall displacement (R_HL_H).

Table 1
Correlation between EC elements and physical parameters

Element	Physical parameter	Comments
R_{DC}	DC resistance	DC resistance of sample
R_s	$\sim 1/\beta_s$	Damping of spin rotation
C_s	$\sim 1/m_{eff}$	Domain wall effective mass
L_s	$\sim(\alpha) \sim \mu_{spin}$	Spin rotation permeability
R_p	$\sim 1/\beta_p$	Damping of wall bulging
L_p	$\sim(\alpha) \sim \mu_{bulg}$	Wall bulging permeability
R_H	$\sim 1/\beta_H$	Damping of domain wall displacement
L_H	$\sim(\alpha) \sim \mu_{displ}$	Domain wall displacement permeability

the correlation between EC elements and physical parameters is shown in Table 1.

5. Conclusions

We have shown that GMI can effectively be modeled by means of an EC, where each section is associated with a particular magnetization process, leading to a resolution of such processes. A correlation between EC elements and physical parameters of the material was proposed. These results could allow the calculation of microscopical parameters from easy, nondestructive macroscopical measurements.

Acknowledgements

This work was funded by DGAPA-UNAM Mexico (grant PAPIIT IN111200).

References

[1] K. Mohri, T. Uchiyama, L.V. Panina, Sensors Actuators A 59 (1997) 1.
[2] M. Vázquez, et al., Sensors Actuators A 59 (1997) 20.
[3] R. Valenzuela, M. Vázquez, A. Hernando, J. Appl. Phys. 79 (1996) 6549.
[4] L.V. Panina, K. Mohri, K. Bushida, M. Noda, J. Appl. Phys. 76 (1996) 6549.
[5] R.S. Beach, A.E. Berkowitz, Appl. Phys. Lett. 64 (1994) 3652.
[6] K.L. García, R. Valenzuela, J. Appl. Phys. 87 (2000) 5257.
[7] E. Carrasco, K.L. García, R. Valenzuela, IEEE Trans. Magn. 34 (1998) 1159.
[8] R. Valenzuela, M. Knobel, M. Vázquez, A. Hernando, J. Appl. Phys. 78 (1995) 5189.
[9] M.T. González, K.L. García, R. Valenzuela, J. Appl. Phys. 85 (1999) 319.
[10] Y. Waseda, S. Ueno, M. Hagiwara, K.T. Austen, Prog. Mater. Sci. 34 (1990) 149.
[11] M.L. Sánchez, R. Valenzuela, M. Vázquez, A. Hernando, J. Mater. Res. 11 (1996) 2486.
[12] P. Ciureanu et al., Proceedings of the Asian-Pacific Microwave Conference, Singapore, Vol. 3, 2000, pp. 876.
[13] M.R. Britel, et al., Appl. Phys. Lett. 77 (2000) 2737.